Supporting Information

Stack-Pressure-Dependent Interfacial Capacitance Governs Electrochemical Contact in All-Solid-State Batteries

Shunsuke Kawaguchi, Hideki Ikekawa, Wataru Ogihara, Minoru Kuzuhara, Takuhiro Miyuki, Yuichi Aihara and Koichiro Aotani*

This file includes Supporting Information, Figures S1–S10 and Tables S1–S10.

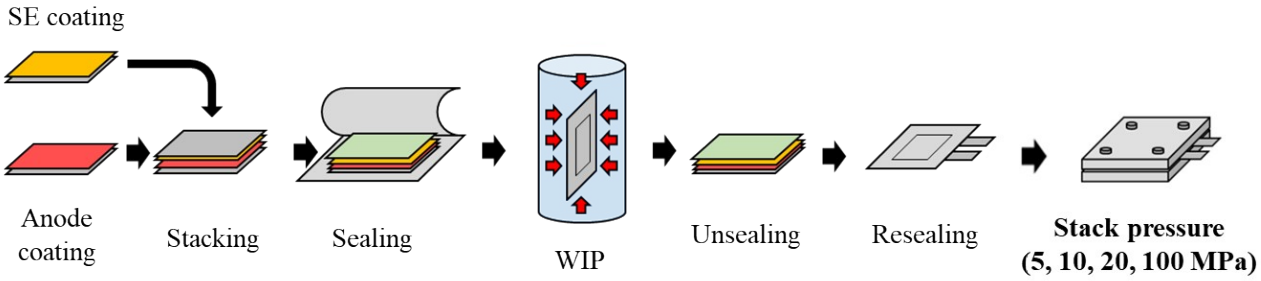

Figure S1 Schematic overview of the full-cell fabrication workflow. Controlled stack pressures (5, 10, 20, and 100 MPa) were exerted through deliberate modulation of the mechanical constraint applied to the assembled cell.

Table S1 Detailed specifications of the all-solid-state battery (ASSB) cell configuration.

	Active Material	Solid electrolyte	Conductive	Binder	Loading weight
Cathode	NCM523	$Li_{7-x}PS_{6-x}Cl_x$	VGCF	SBR	20.0 mg cm^{-2}
	82.7 wt.%	15.4 wt.%	1.1 wt.%	0.8 wt.%	
Anode	Gr	$Li_{7-x}PS_{6-x}Cl_x$	-	SBR	16.2 mg cm^{-2}
	67.5 wt.%	30.6 wt.%	1.9 wt.%	0.8 wt.%	

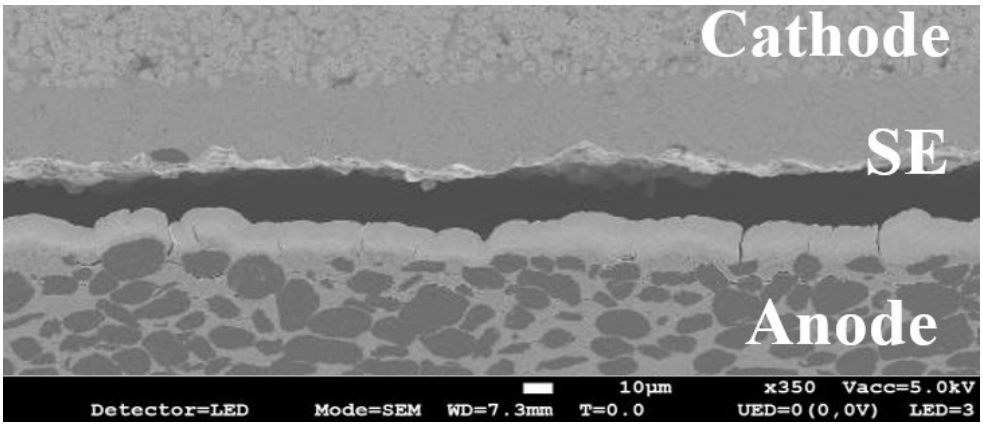

Figure S2 Cross-sectional SEM image of the cell in the fully discharged state after 300 cycles at a charge/discharge rate of 1C/1C under a stack pressure of 5 MPa at 25 °C. The cell cross-section was prepared using a JEOL IB-09020CP cross-section polisher under the following conditions: an accelerating voltage of 5.0 kV, Ar gas flow rate of 5.6, temperature of −40 °C, and milling time of 8 h. As shown in the figure, delamination of the SE layer along the in-plane direction was observed in the vicinity of the negative electrode, together with traces of Li deposition.

Table S2 Detailed specifications of the liquid-based batteries (LIB) cell configuration.

	Active Material	Electrolyte	Conductive	Binder	Loading weight
Cathode	NCM523	PP separator	VGCF+AB	PVdF	20 mg cm^{-2}
	94 wt.%	1 M $LiPF_6$ in an EC:EMC mixture at 1:3 volume ratio, with 2 wt.% VC	3 wt.%	3 wt.%	
Anode	Gr		VGCF	CMC+SBR	16.2 mg cm^{-2}
	93 wt.%		4 wt.%	3 wt.%	

Table S3 Specifications of the cathode symmetric cells in liquid-based batteries (LIB) and ASSB.

	LIB	**ASSB**
	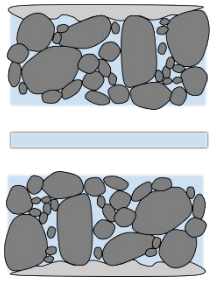	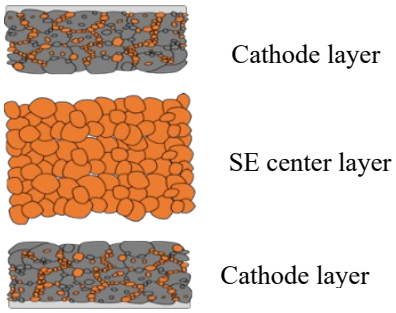
Upper layer	Foil : C-coated Al foil (10 μm) NCM523 : SE : VGCF : binder (82.7 : 0 : 1.1 : 0.8 wt.%) Loading : 22.5 mg/cm^2 Thickness : ~80 μm Press : Roll press	Foil : C-coated Al foil (10 μm) NCM523 : SE : VGCF : binder (82.7 : 15.4 : 1.1 : 0.8 wt.%) Loading : 23.0 mg/cm^2 Thickness : ~70 μm Press : WIP
Center layer	PP separator (10 μm) Press : No	Foil : No SE : binder (98 : 2 wt.%) Loading : 5 mg/cm^2 Thickness : ~50 μm Press : WIP
Lower Layer	Foil : C-coated Al foil (10 μm) NCM523 : SE : VGCF : binder (82.7 : 0 : 1.1 : 0.8 wt.%) Loading : 22.5 mg/cm^2 Thickness : ~80 μm Press : Roll press	Foil : C-coated Al foil (10 μm) NCM523 : SE : VGCF : binder (82.7 : 15.4 : 1.1 : 0.8 wt.%) Loading : 23.0 mg/cm^2 Thickness : ~70 μm Press : WIP

Table S4 Specifications of the anode symmetric cells in liquid-based batteries (LIB) and ASSB.

	LIB	**ASSB**
		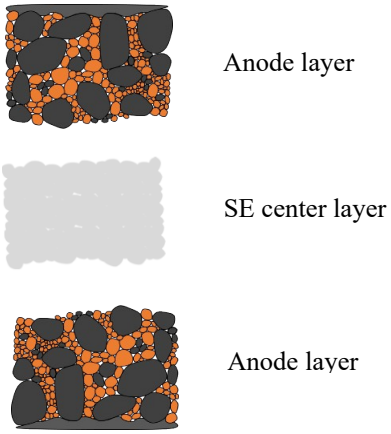
Upper layer	Foil : C-coated SUS foil (10 μm) Graphite : SE : binder (67.5 : 0 : 1.9 wt.%) Loading : 16.5 mg/cm^2 Thickness : ~80 μm Press : Roll press	Foil : C-coated SUS foil (10 μm) Graphite : SE : binder (67.5 : 30.6 : 1.9 wt.%) Loading : 18.0 mg/cm^2 Thickness : ~90 μm Press : WIP
Center layer	PP separator (10 μm) Press : No	Foil : No SE : binder (98 : 2 wt.%) Loading : 5 mg/cm^2 Thickness : ~50 μm Press : WIP
Lower Layer	Foil : C-coated SUS foil (10 μm) Graphite : SE : binder (67.5 : 0 : 1.9 wt.%) Loading : 16.5 mg/cm^2 Thickness : ~80 μm Press : Roll press	Foil : C-coated SUS foil (10 μm) Graphite : SE : binder (67.5 : 30.6 : 1.9 wt.%) Loading : 18.0 mg/cm^2 Thickness : ~90 μm Press : WIP

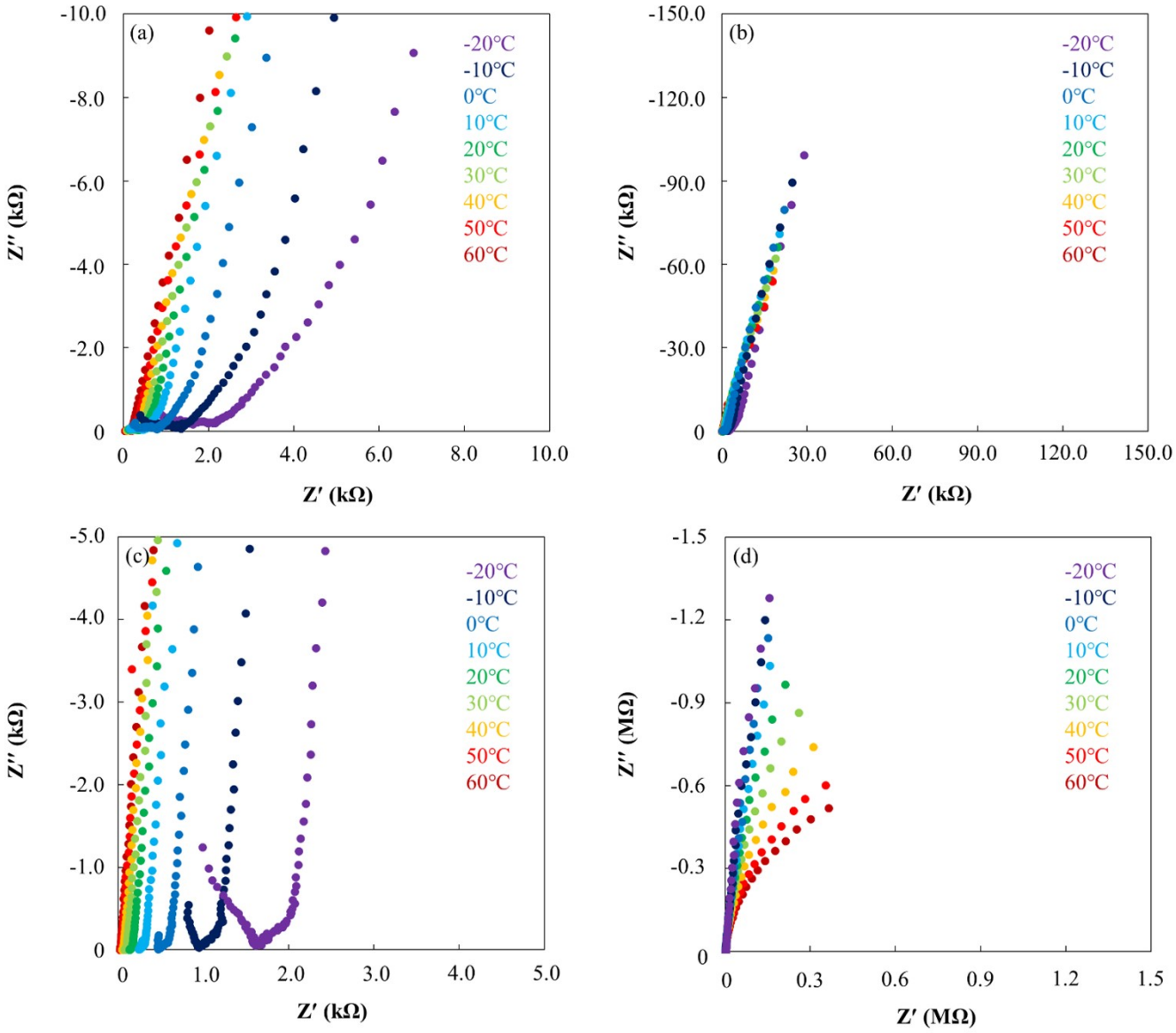

Figure S3 Nyquist plots of the cathode layer/SE layer/cathode layer and anode layer/SE layer/anode layer symmetric cells measured from −20 to 60 °C, as shown in Fig. 2 of the main text. The equivalent circuits used for fitting the respective symmetric cells are presented in Figure S5, and the fitting parameters are summarized in Tables S5 and S6. In addition, representative fitting residuals at −20, 20, and 60 °C are extracted and shown in Fig. S6.

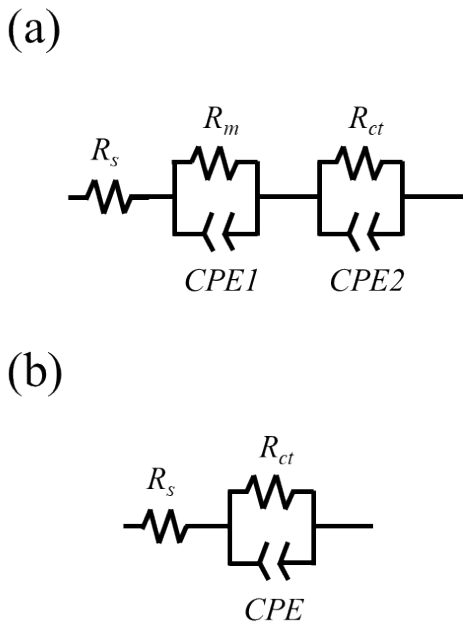

Figure S4 Equivalent circuits for the symmetric cells employing (a) cathode layer/SE layer/cathode layer and (b) anode layer/SE layer/anode layer configurations. R_s represents the contact resistance in the cell, R_m represents the resistance originating from the coating-layer component in the cathode layer, and R_{ct} represents the charge-transfer resistance at the active material/SE interface. *CPE* represents the pseudo-capacitive component associated with each resistance element.

Table S5 List of fitting parameters for the cathode layer/SE layer/cathode layer symmetric cell corresponding to Fig. 2.

Temperature	R_s	R_m	$\alpha 1$	R_{ct}	$\alpha 2$
-20℃	1.7×10^{3} Ω	2.2×10^{3} Ω	0.82	1.1×10^{5} Ω	0.85
-10℃	9.5×10^{2} Ω	1.4×10^{3} Ω	0.81	1.0×10^{5} Ω	0.84
0℃	4.5×10^{2} Ω	8.3×10^{2} Ω	0.80	9.3×10^{4} Ω	0.86
10℃	2.4×10^{2} Ω	6.5×10^{2} Ω	0.83	8.7×10^{4} Ω	0.86
20℃	1.5×10^{2} Ω	4.0×10^{2} Ω	0.82	8.4×10^{4} Ω	0.87
30℃	8.8×10^{1} Ω	2.4×10^{2} Ω	0.81	8.1×10^{4} Ω	0.86
40℃	6.6×10^{1} Ω	1.0×10^{2} Ω	0.80	7.8×10^{4} Ω	0.88
50℃	4.1×10^{1} Ω	7.4×10^{1} Ω	0.82	7.3×10^{4} Ω	0.87
60℃	2.4×10^{1} Ω	5.5×10^{1} Ω	0.81	6.9×10^{4} Ω	0.88

Table S6 List of fitting parameters for the Anode layer/SE layer/Anode layer symmetric cell corresponding to Fig. 2.

Temperature	R_s	R_{ct}	α
-20℃	1.7×10^{3}	6.6×10^{6}	0.91
-10℃	9.5×10^{2}	6.2×10^{6}	0.90
0℃	4.5×10^{2}	5.8×10^{6}	0.92
10℃	2.4×10^{2}	5.4×10^{6}	0.92
20℃	1.5×10^{2}	5.0×10^{6}	0.93
30℃	8.3×10^{1}	4.6×10^{6}	0.93
40℃	6.6×10^{1}	4.2×10^{6}	0.94
50℃	3.9×10^{1}	3.9×10^{6}	0.95
60℃	2.1×10^{1}	3.6×10^{6}	0.96

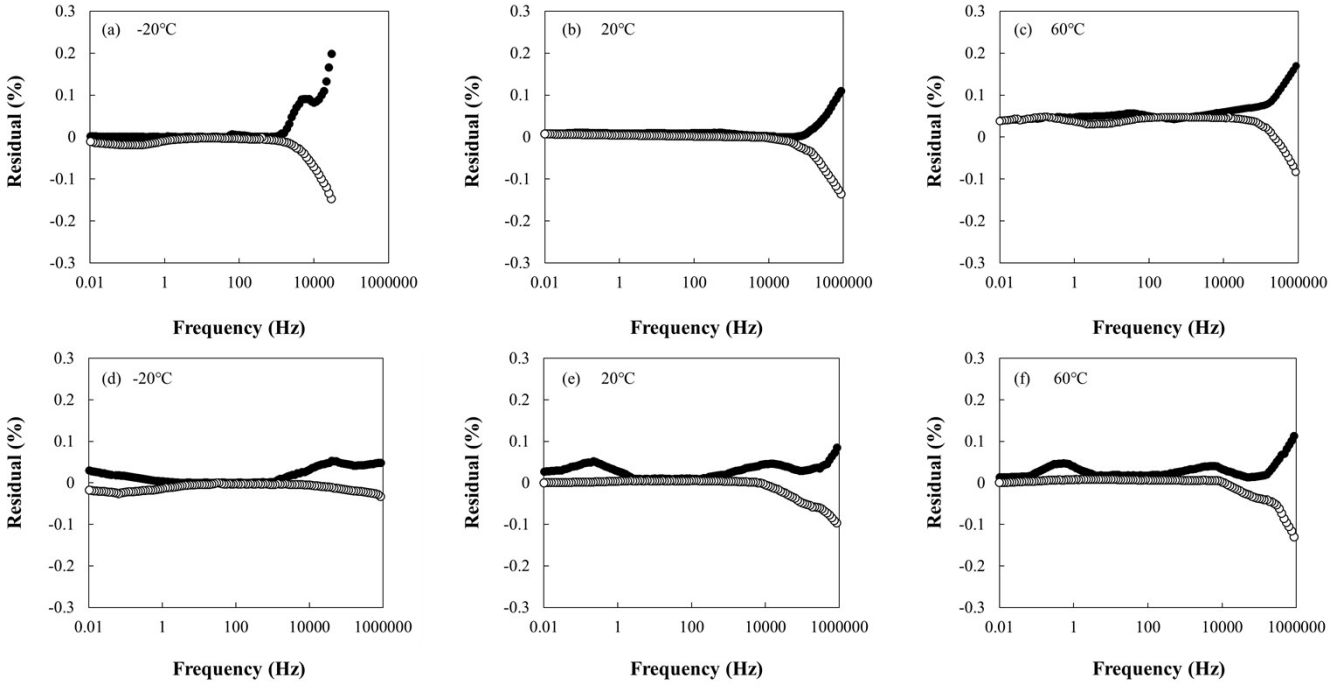

Figure S5 Relative errors for the fitting of the Nyquist plots of the symmetric cells using the anode layer/SE layer/anode layer and cathode layer/SE layer/cathode layer configurations shown in Fig. 2, plotted as a function of measurement frequency. The relative differences between the experimental and fitted values for the real and imaginary components of the Nyquist plots are presented. Panels (a)–(c) show the results for the anode layer/SE layer/anode layer symmetric cell at −20, 20, and 60 °C, respectively, while panels (d)–(f) show the corresponding results for the cathode layer/SE layer/cathode layer symmetric cell.

Table S7 Active material fraction and corresponding effective specific surface area in the cathode and anode composites for ASSBs and LIBs. The effective specific surface area was calculated assuming spherical particle geometry.

	D_{50} of the active material (μm)	Ratio of the active material (vol %)	Total surface area of active materials in the electrode (cm^2)
Cathode (ASSB)	5.0	56.0	37.8
Cathode (LIB)	↑	63.7	43.0
Anode (ASSB)	16.0	50.0	11.5
Anode (LIB)	↑	68.9	15.8

Table S8 List of dielectric constants for the materials used in this study. The dielectric constant values were taken from the references listed in the table.

Geometrically estimated interfacial capacitance derived from

$C = \varepsilon_0 \varepsilon_r A/d$,

using literature-reported dielectric constants (ε_r), BET-derived effective interfacial areas (A), and an assumed interfacial charge-separation distance d of 2 nm.

Materials	**ε_r**	**References**
$LiNbO_3$	~30	[1]
$LiNi_{0.5}Mn_{0.2}Co_{0.3}O_2$	~15	[2]
Graphite	~10	[3]
Li_6PS_5Cl	~12	[4]
Li_3PS_4-x$LiBH_4$	~15	[5]
$LiPF_6$ EC:DEC	~40	[6]

Table S9 Correlation between LPSBH particle size (D_{50}) and wet -milling conditions used for particle size reduction.

Particle size (D_{50})	Milling condition					Solvent condition			
	Ball size (mm)	Ball amount (g)	Ball type	Speed (rpm)	Time (h)	Solvent i	Solvent ii	Ratio (i/ii)	Amount (g)
10.2	10.0	440	ZrO_2	60	2	heptane	dibutyl ether	4:1	250
5.3	5.0	↑	↑	↑	4	↑	↑	↑	↑
1.2	1.0	↑	↑	↑	10	↑	↑	↑	↑
0.4	0.65	↑	↑	↑	↑	↑	↑	↑	↑

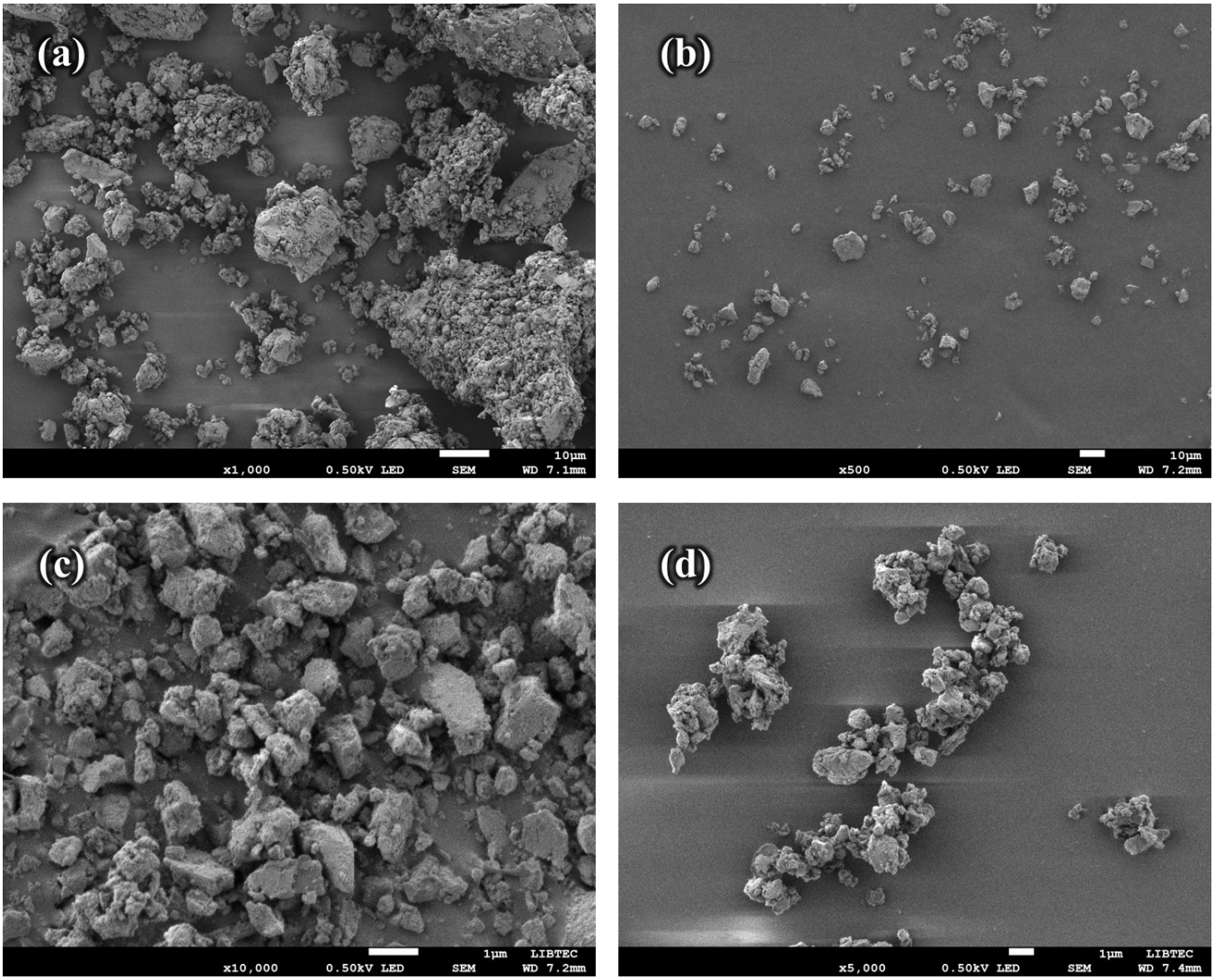

Figure S6 Correlation between LPSBH particle size and the corresponding SEM images. Particle size reduction was performed under the conditions summarized in Table S9. After milling, the SE powders were characterized by SEM, and the particle size (D_{50}) was determined by image analysis of at least 1000 individually distinguishable particle agglomerates dispersed on the sample stage. Each SEM image shows the observed morphology of SE particles with (a) D_{50} = 10.2 µm, (b) D_{50} = 5.3 µm, (c) D_{50} = 1.2 µm, and (d) D_{50} = 0.4 µm, respectively.

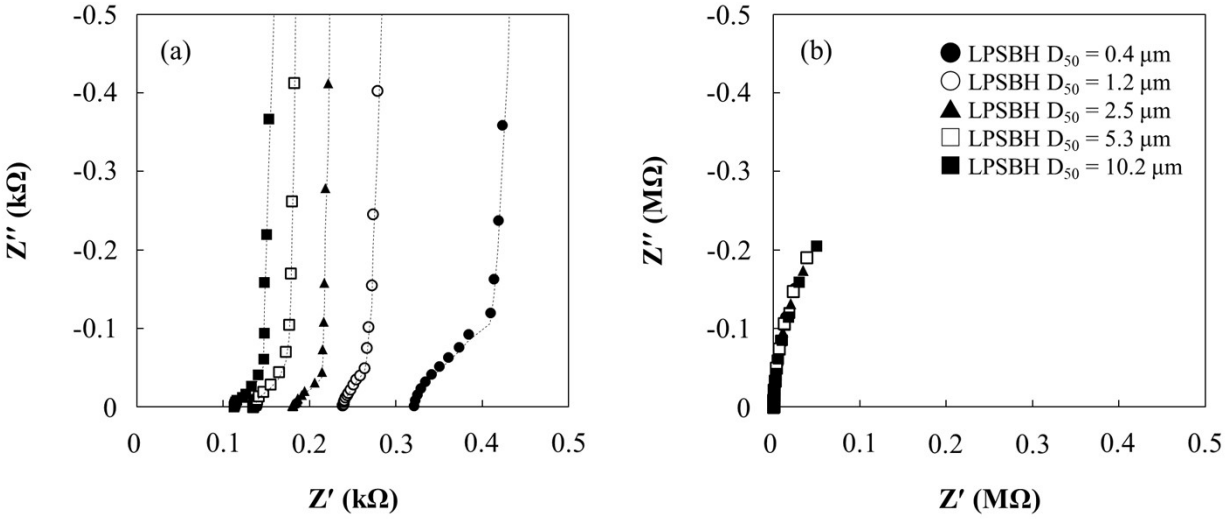

Figure S7 Nyquist plots at 20 °C for anode layer/SE layer/anode layer symmetric cells employing LPSBH solid electrolytes pulverized under different conditions, corresponding to Fig. 5. The fitting parameters for the measured results are summarized in Table S10, and the relative errors between the experimental and fitted values are shown in Figure S8.

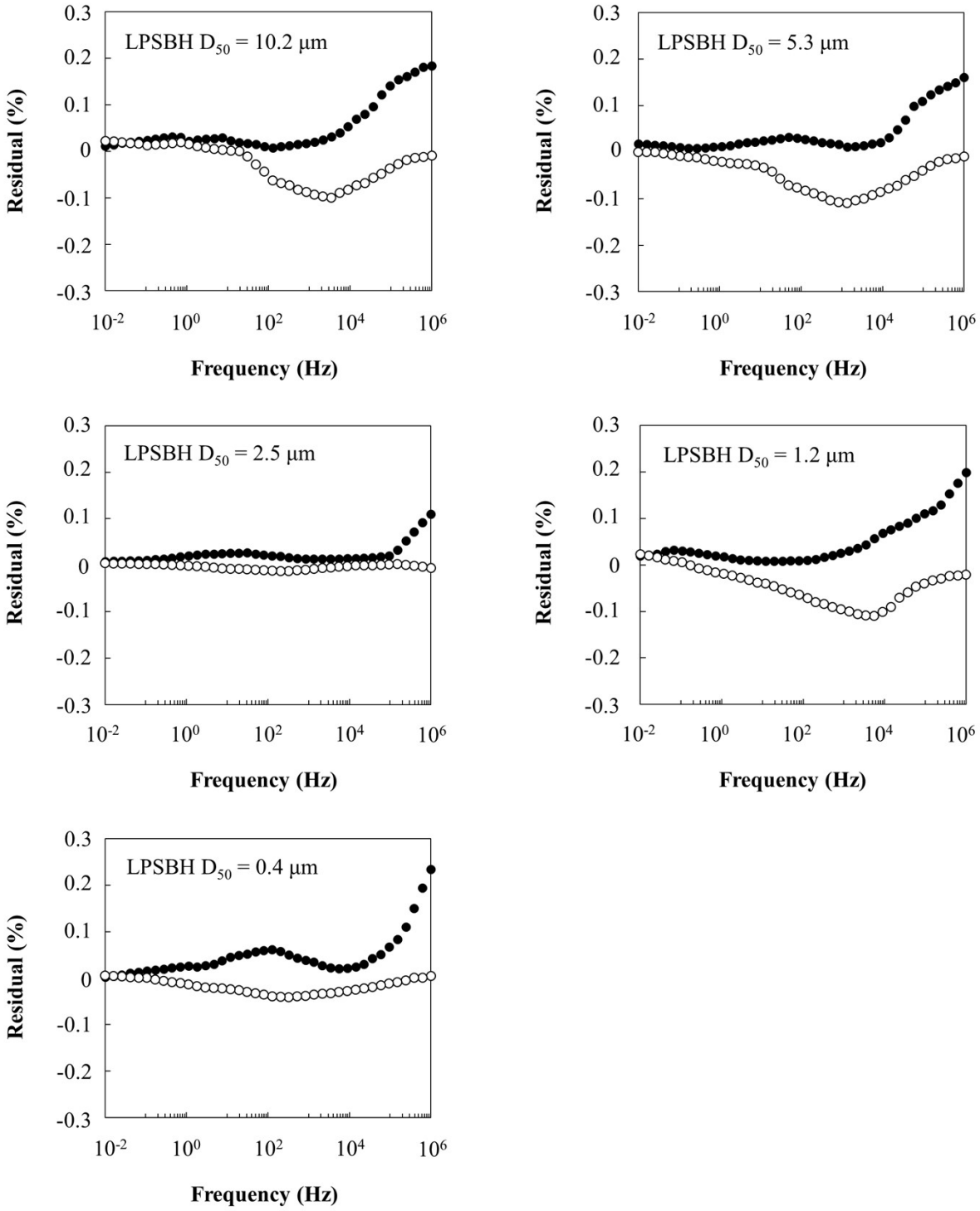

Figure S8 Relative residuals for the fitting of the Nyquist plots of the anode layer/SE layer/anode layer symmetric cells shown in Figure 5, plotted as a function of measurement frequency. The relative differences between the experimental and fitted values for the real and imaginary components of the Nyquist plots are presented.

Table S10 List of fitting parameters for the anode layer/SE layer/anode layer symmetric cells corresponding to Fig. 5.

Particle size	R_s	R_{ion}	R_{ct}	α
0.4 μm	$3.2\times10^{2}\ \Omega$	$4.0\times10^{2}\ \Omega$	$6.5\times10^{5}\ \Omega$	0.91
1.2 μm	$2.4\times10^{2}\ \Omega$	$2.8\times10^{2}\ \Omega$	$5.2\times10^{5}\ \Omega$	0.92
2.5 μm	$1.8\times10^{2}\ \Omega$	$2.1\times10^{2}\ \Omega$	$7.5\times10^{5}\ \Omega$	0.93
5.3 μm	$1.4\times10^{2}\ \Omega$	$1.7\times10^{2}\ \Omega$	$9.1\times10^{5}\ \Omega$	0.93
10.2 μm	$1.1\times10^{2}\ \Omega$	$1.3\times10^{2}\ \Omega$	$1.5\times10^{6}\ \Omega$	0.94

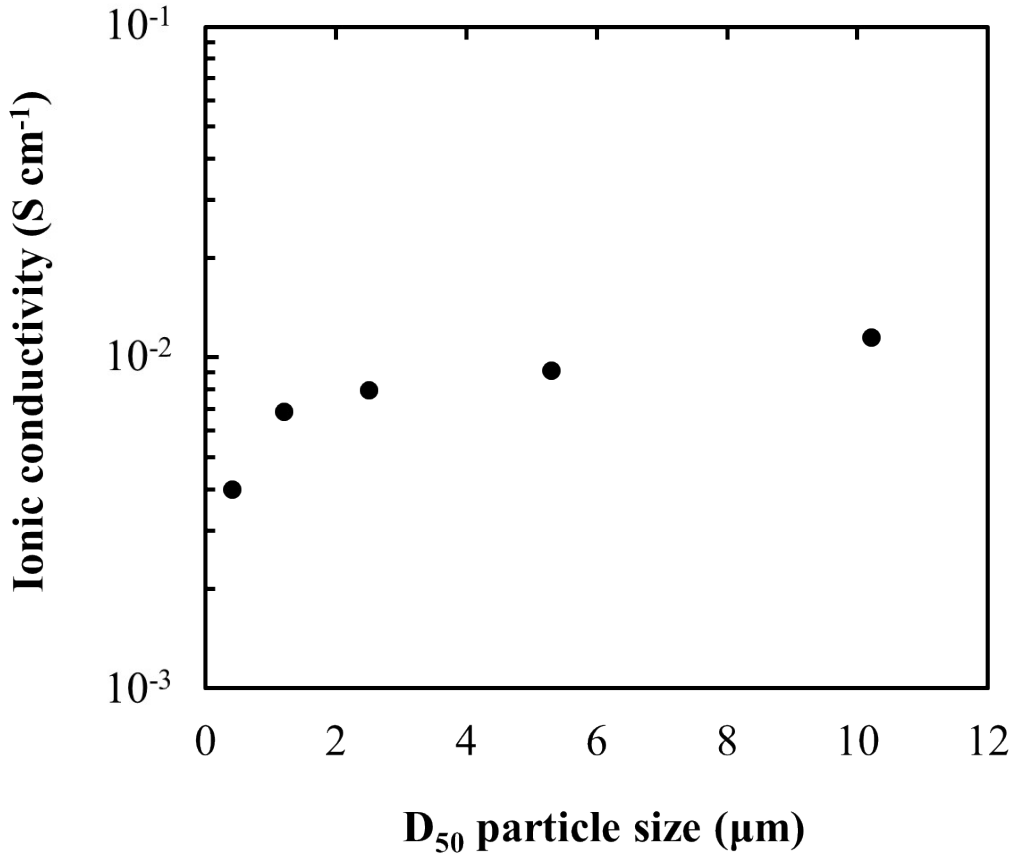

Figure S9 Correlation between LPSBH particle size (D_{50}) and ionic conductivity. Ionic conductivity was determined by electrochemical impedance spectroscopy after pellet fabrication via pre-pressing at 100 MPa followed by main pressing at 600 MPa for 1 min, ensuring sufficient densification of 100 mg SE powders sandwiched between SUS current collectors.

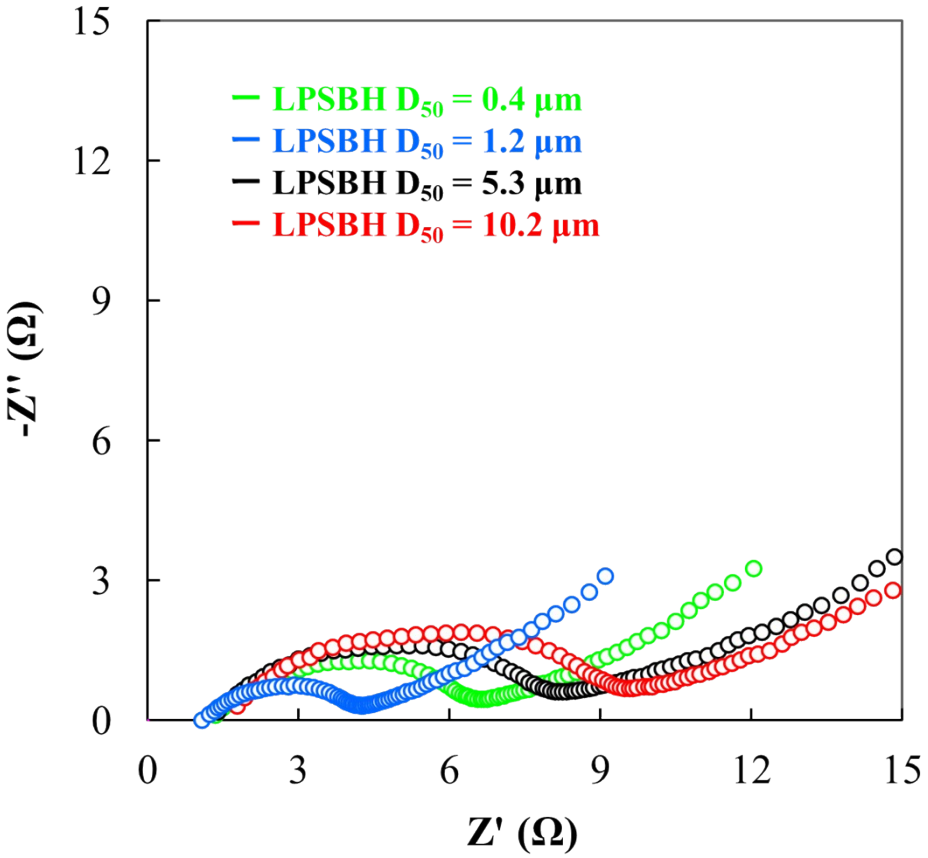

Figure S10 Correlation between LPSBH particle size in the anode composite layer and full-cell impedance spectra. EIS was conducted at room temperature after three formation cycles at 0.1C/0.1C. The cells were subsequently charged to 50% state of charge (SOC) at 0.1C/0.1C, rested for 8 h to ensure voltage stabilization, and then subjected to impedance measurements.

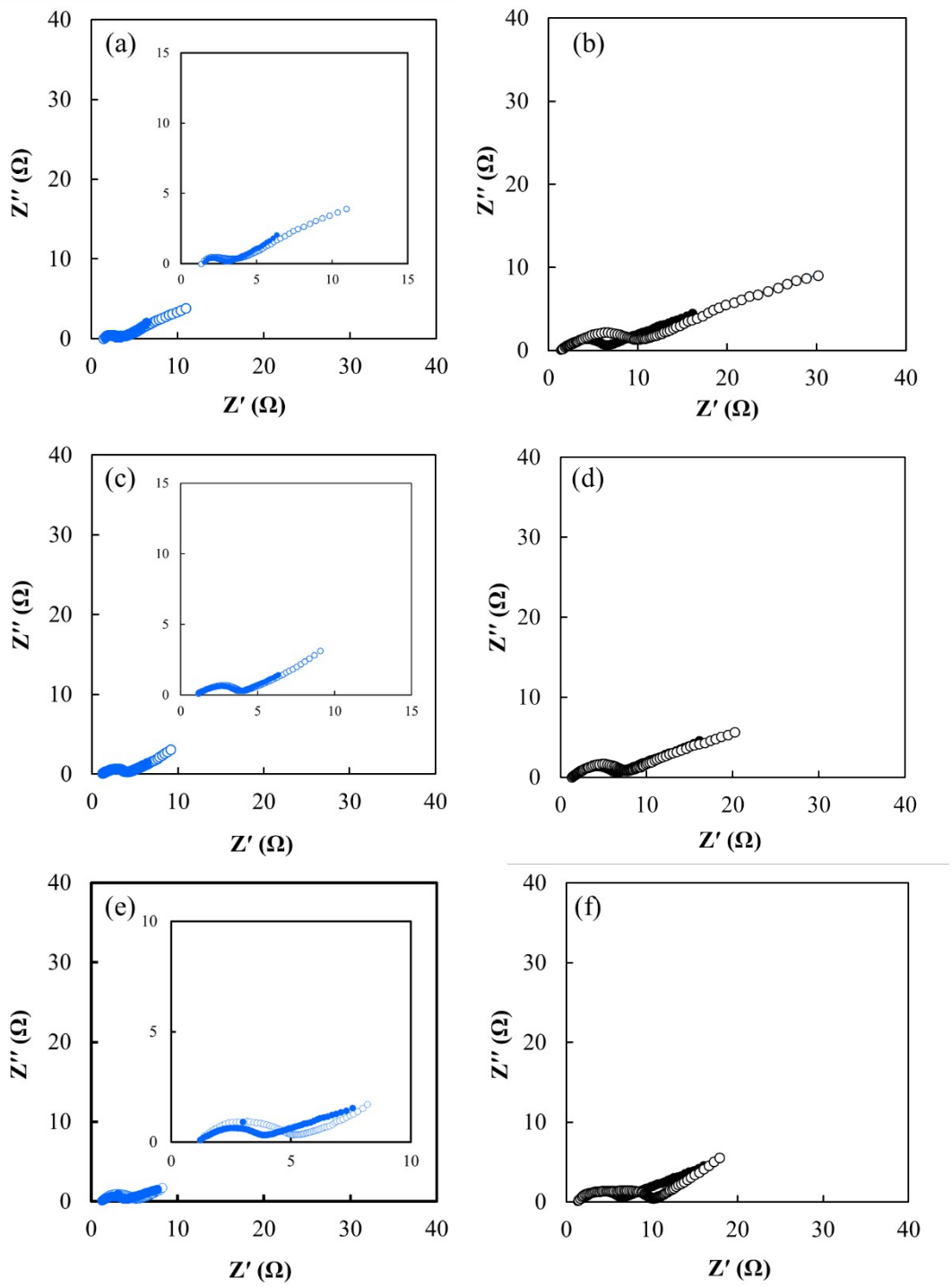

Figure S11 Evolution of the EIS behavior during cycling tests of full cells employing LPSBH solid electrolytes with D_{50} values of 5.3 µm (black) and 1.2 µm (blue) in the anode layer, corresponding to Fig. 7. Filled symbols represent the results measured before cycling, while open symbols represent the results obtained after 300 cycles at 1C/1C and after 30 cycles at 0.1C/0.1C. EIS measurements were conducted at the voltage corresponding to SOC 50% based on the cell capacity, over a frequency range from 10 mHz to 1 MHz with an AC amplitude of 10 mV. (a,b) Results for 1C/1C cycling at 5 MPa; (c,d) results for 1C/1C cycling at 20 MPa; and (e,f) results for 0.1C/0.1C cycling at 5 MPa.

References

[1] R. Schmutzler et al., *Ferroelectrics*, 1980, **32**, 125–128.

[2] J. Jamnik & J. Maier, *Phys. Chem. Chem. Phys*., 2001, **3**, 1668–1678.

[3] H. Ohta et al., *Carbon*, 1994, **32**, 1241–1249.

[4] A. Kraft et al., *Journal of the American Ceramic Society*, 2017, **100**, 3563–3574.

[5] T. Ikeshoji & S. Orimo et al., *Appl. Phys. Lett.*, 2013, **103**, 133903.

[6] M. Ue, *Journal of The Electrochemical Society*, 1994, **141**, 3336–3342.